Neutron densities and the equation of state for neutron-rich matter

D. Alonso and F. Sammarruca
Physics Department, University of Idaho, Moscow, Idaho 83844, USA
(Received 1 July 2003; published 13 November 2003)

We present predictions for energies, proton and neutron rms radii, and neutron skins of some closed-shell nuclei based upon a microscopic model of the equation of state for asymmetric nuclear matter which is used as input for a mass formula. We employ realistic two-body forces and the Dirac-Brueckner-Hartree-Fock approach to nuclear matter. We compare with experimental information, when available, and point out the need for accurate determinations of neutron densities and skins.

DOI: 10.1103/PhysRevC.68.054305 PACS number(s): 21.65.+f, 21.10.Dr, 21.10.Gv

I. INTRODUCTION

One of the main challenges in nuclear physics is to understand how the properties of nuclei arise from the interactions among the protons and the neutrons.

The ability to vary the ratio between protons and neutrons over a large range is a crucial tool to reach that understanding, but has so far been rather limited. The advent of beams of short-lived, radioactive nuclei promises to change this situation, providing new opportunities to explore unknown regions and possibly phenomena and symmetries different from those seen in the stability region. If approved for construction, the Rare Isotope Accelerator (RIA) will allow the study of unique nuclear systems which are expected to exist at the boundaries of the nuclear chart.

Furthermore, studies of the strong interactions between protons and neutrons in exotic matter are important for our understanding of astrophysical processes, such as structure of neutron stars and what supports them against gravitational collapse. Thus, it is important and timely to develop microscopic effective interactions which can account for the asymmetry between proton and neutron densities.

Neutron skins are crucial observables and may have impact on phenomena such as phase transitions inside a neutron star. Recent calculations by Horowitz and Piekarewicz [1] have suggested a relation between the skin of a heavy nucleus and the properties of neutron star crusts. A softer symmetry energy implies larger central densities and thus smaller radii. However, although a strong correlation is found between skin thickness and star radius, the latter is not uniquely constrained by a measurement of the neutron skin, because the skin depends on the equation of state (EOS) at or below saturation density, while the star radius is also sensitive to the high density behavior of the EOS. Separate measurements of the two could provide valuable information on the EOS at low and high densities [1].

Our knowledge of matter distribution inside asymmetric nuclei must be improved and broadened. The doubly magic nucleus ^{208}Pb is perhaps one of the most asymmetric nuclei for which a considerable database exists. Nevertheless, determinations of neutron densities differ considerably depending on the model used in the analysis [2], while almost nothing is known about much more neutron-rich nuclei.

The recent analysis by Clark *et al.* [3] finds values of neutron rms radii and neutron skins generally not in agreement with those predicted by relativistic mean-field models, which are typically larger. In Ref. [4], Furnstahl investigates the spread in neutron skin predictions for ^{208}Pb within mean-field models. The nature of that variation is studied using correlations between basic properties of the models and neutron skin thickness in ^{208}Pb. The results suggest that mean-field models may overestimate the skin thickness and that additional constraints may be needed to improve the model functionals [4].

Phenomenological EOS based on the nonrelativistic Skyrme Hartree-Fock theory and the relativistic mean-field theory, respectively, have been used to predict neutron skins of Na isotopes [5]. When compared with the available data [6], which carry considerable uncertainties, the two calculations appear to be the two extreme cases bounding a region consistent with experiment.

In a previous work [7], we presented microscopic calculations of the equation of state for asymmetric matter. We used realistic nucleon-nucleon (*NN*) forces and the Dirac-Brueckner-Hartree-Fock (DBHF) framework. We also calculated properties of astrophysical significance, such as the pressure in symmetric matter and neutron matter up to about five times the saturation density, and compared with recent experimental constraints obtained from analyses of nuclear collisions [8].

Following that work, the purpose of this paper is to present predictions for energies, proton and neutron radii, and neutron skins of finite nuclei based upon the EOS. We will use a liquid droplet model, which, in spite of its simplicity, provides a useful mean to relate the EOS directly to structural properties of nuclei, thus allowing a study of the sensitivity of those properties to the EOS model.

In Sec. II, we describe our calculations (Sec. II A) and present results obtained with three relativistic potentials and the DBHF framework (Sec. II B). For comparison, we also present a sample of predictions obtained within the nonrelativistic context of conventional Brueckner theory (Sec. II C). Our predictions are a direct reflection of the EOS which, in turn, is determined by the nature of the two-body force as well the chosen many-body methods. In Sec. II D, we take a critical look at both of these aspects. Section III contains our conclusions and related future plans.

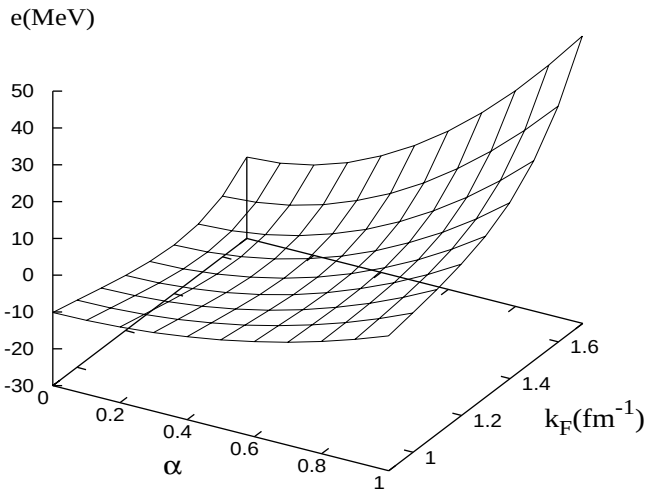

FIG. 1. Energy per nucleon e as a function of the Fermi momentum k_F and the neutron excess parameter α.

II. EOS-BASED PREDICTIONS OF NUCLEAR ENERGIES AND RADII

A. Description of the calculation

Asymmetric (infinite) nuclear matter can be characterized by the neutron density ρ_n and the proton density ρ_p. It is also convenient to define the total density $\rho=\rho_n+\rho_p$ and the asymmetry (or neutron excess) parameter $\alpha=(\rho_n-\rho_p)/\rho$. Clearly, $\alpha=0$ corresponds to symmetric matter, and $\alpha=1$ to neutron matter.

The average Fermi momentum is related to the total density in the usual way,

$$\rho=\frac{2k_F^3}{3\pi^2}. \tag{1}$$

The EOS, or energy per nucleon as a function of density, is defined as

$$\bar{e}(\rho_n,\rho_p)=\frac{\rho_n\bar{e}_n+\rho_p\bar{e}_p}{\rho} \tag{2}$$

or

$$\bar{e}(k_F,\alpha)=\frac{(1+\alpha)\bar{e}_n+(1-\alpha)\bar{e}_p}{2} \tag{3}$$

with $\bar{e}_{n/p}$, the energy per neutron/proton.

Figure 1 provides a three-dimensional view of the equation of state, shown as a function of the neutron excess parameter and the average Fermi momentum. The two-body interaction used for that figure is the Bonn B potential (used within the relativistic Thompson scattering equation [9]). Details of the calculation are reported in Ref. [7].

We expect the relation between energies and radii to be sensitive to the details of the EOS. How the energy moves up as a function of α and how the minimum shifts towards lower densities for increasing neutron fraction will determine the most stable configuration predicted for the nucleus under consideration, as well as variations of the central density for increasing number of neutrons. To which extent excess neutrons are pushed out to diffuse the neutron surface thus developing a neutron skin will clearly reflect the saturation density of asymmetric matter.

A relatively straightforward way to relate the microscopic EOS directly to structural properties of finite nuclei is a simple liquid droplet model [5], where the "volume" term is directly related to the EOS. Schematically, one may write the energy of a nucleus in terms of a mass formula

$$E=\int_0^\infty \bar{e}[\rho_n(r),\rho_p(r)]\rho(r)4\pi r^2dr+\int_0^\infty f_0|\nabla\rho(r)|^2 4\pi r^2dr + \frac{e^2}{4\pi\epsilon_0}(4\pi)^2\int_0^\infty dr' r'\rho_p(r')\int_0^{r'} dr\rho_p(r)r^2, \tag{4}$$

where the last two terms on the right-hand side are the surface energy and the Coulomb energy, respectively. The latter is calculated integrating the electrostatic interaction between a uniformly charged sphere of radius r' and a uniformly charged spherical shell of thickness dr'. The constant f_0 is taken to be 70 MeV fm^5 from fits to binding energies and radii of β-stable nuclei [10]. The integrand in the first term contains precisely the EOS for asymmetric matter. The proton and neutron densities, or, equivalently, the total density $\rho(r)=\rho_n(r)+\rho_p(r)$ and the neutron excess parameter $\alpha(r)=[\rho_n(r)-\rho_p(r)]/\rho(r)$, are now functions of the radial coordinate.

One can then parametrize the proton and neutron density functions and search for the values of those parameters that maximize the binding energy of the nucleus. We have used standard two-parameter Fermi distributions, that is,

$$\rho_i(r)=\frac{a_i}{1+e^{(r-b_i)/c_i}}, \tag{5}$$

with $i=n,p$ for neutron/proton, respectively. The parameters b_i and c_i are the radius and diffuseness, and the value of a_i is determined by normalizing the density distributions to N or Z. For each set of trial parameters, the functions $\rho(r)$ and $\alpha(r)$ are evaluated over the integration range, and the EOS from Fig. 1 is interpolated as a function of two variables. Alternatively, we can save one interpolation by writing the EOS as an analytical function of α [7]

$$\bar{e}(\rho,\alpha)-\bar{e}(\rho,0)=e_s(\rho)\alpha^2, \tag{6}$$

with e_s the symmetry energy. We observed no significant differences in the results when using Eq. (6) to represent the EOS for any α.

B. Results with DBHF-based EOS

The energy per particle obtained from Eq. (4) are shown in Table I for some magic or semimagic nuclei. We have considered ^{40}Ca as a nucleus with $N=Z$, two cases with different levels of asymmetry, ^{90}Zr and ^{208}Pb (average asymmetry parameter $(N-Z)/A$ equal to 0.11 and 0.21, respectively), and the more strongly asymmetric ^{266}Pb for which no experimental information is available, but which could be doubly

TABLE I. Binding energy/particle (in MeV) obtained with three relativistic potentials.

Nucleus	Binding energy (expt.)	Potential	Binding energy
		Bonn *A*	9.23
^{40}Ca	8.55	Bonn *B*	8.44
		Bonn *C*	7.99
		Bonn *A*	9.70
^{90}Zr	8.71	Bonn *B*	8.74
		Bonn *C*	8.18
		Bonn *A*	8.97
^{208}Pb	7.87	Bonn *B*	7.95
		Bonn *C*	7.35
		Bonn *A*	7.81
^{266}Pb		Bonn *B*	6.92
		Bonn *A*	6.41

magic [11]. The binding energy per particle for this nucleus predicted with a phenomenological Skyrme interaction is 6.669 MeV [11].

We have used three relativistic one-boson-exchange potentials, the Bonn *A*, *B*, and *C* potentials. In all cases, the EOS to be used in Eq. (4) is obtained in a DBHF calculation of infinite nuclear matter. As is well known, Bonn *A* is the most attractive among the three potentials [9]. This behavior is related to the strength of the tensor force, which contributes to nuclear matter binding through second-order contributions to the central force. As a consequence of that, a weaker tensor force implies a larger central force and thus larger binding. In all cases (where experimental information is available), the Bonn *B* predictions appear to be the best (this point will be revisited in Sec. II D), with the significant model dependence reflecting the different saturation energies predicted by the three potentials. These are shown in Fig. 2, where the EOS as a function of the average Fermi momentum is displayed for the three potentials at two values of α. The purpose of the figure is to show how the differences among the three curves decrease as the proton fraction decreases, and become very small in the limit of neutron matter. This is because, as we pointed out above, the tensor force is the major source of model dependence among these potentials. Clearly, the tensor force is mostly reflected in the $^3S_1$ partial wave, which, as a $T=0$ contribution, will lose strength when the system approaches neutron matter.

Figures 3–6 show the predicted proton and neutron point density distributions for the nuclei in Table I obtained with Bonn *A*, *B*, and *C*. Consistent with the observations made above, the model dependence is strongest in the central region [where $\alpha(r)$ is generally small].

In order to compare with the experimental charge radii, our predicted point proton density is folded with the proton charge form factor to yield the charge density through the usual convolution integral,

$$\rho_{ch}(r) = \int d^3r' g(\vec{r} - \vec{r}')\rho_p(r'), \tag{7}$$

where g is the proton charge form factor which is taken to be of Gaussian shape [12],

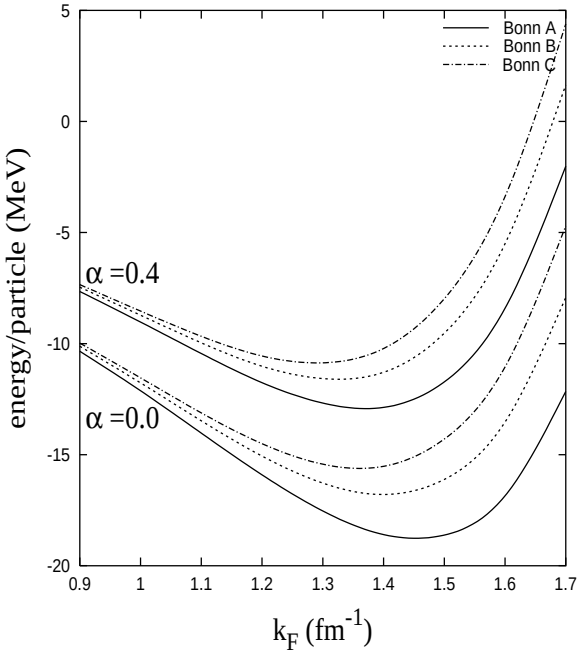

FIG. 2. Energy/nucleon as a function of the Fermi momentum predicted with Bonn *A* (solid line), Bonn *B* (dotted line), and Bonn *C* (dash-dot), for $\alpha=0$ (lower group) and $\alpha=0.4$ (upper group).

$$g(r) = (a\sqrt{\pi})^{-3}e^{-r^2/a^2}, \tag{8}$$

and the constant a is related to the charge radius of the proton (equal to 0.8 fm) through $r_{ch,p}=\sqrt{(2/3)}a$.

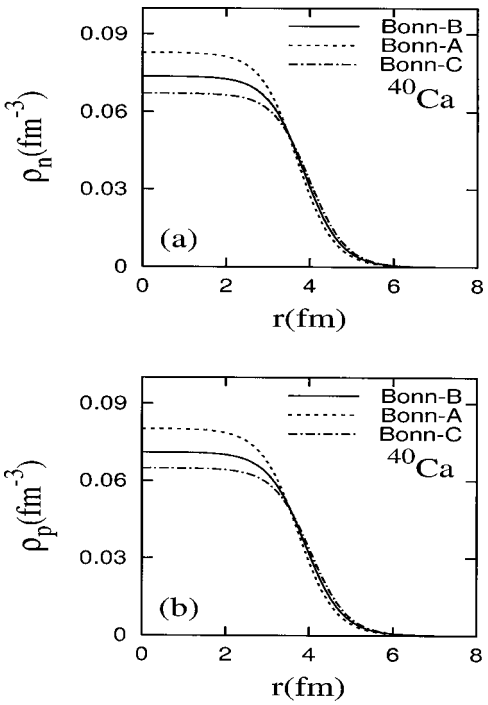

FIG. 3. Neutron (a) and proton (b) density distributions for ^{40}Ca obtained with three relativistic one-boson-exchange potentials. All calculations are DBHF.

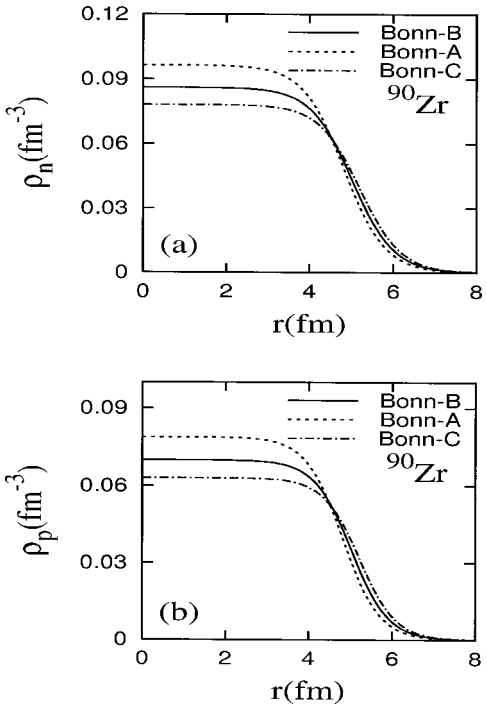

FIG. 4. As in Fig. 3, for ^{90}Zr.

Figures 7–9 show predictions for the rms charge radius, the neutron rms radius, and the neutron skin. The latter is calculated as the difference between the *point* neutron and proton rms radii.

As observed with the energies, the best agreement with the charge radii is obtained with Bonn *B*. The predicted radii getting larger from Bonn *A* to Bonn *C* is again a reflection of the larger attraction generated by the former.

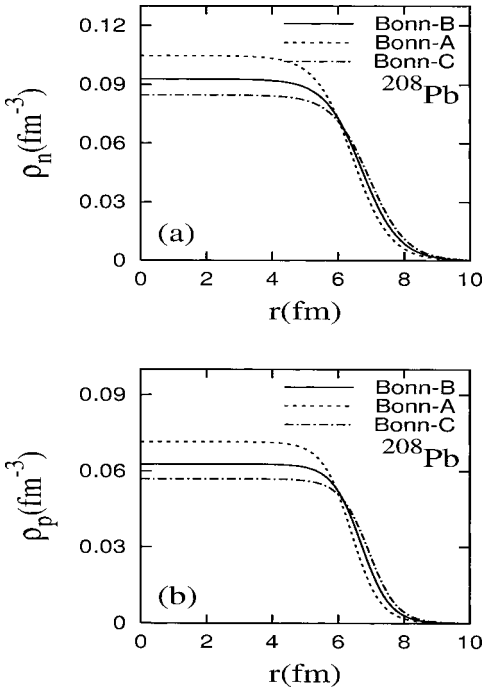

FIG. 5. As in Fig. 3, for ^{208}Pb.

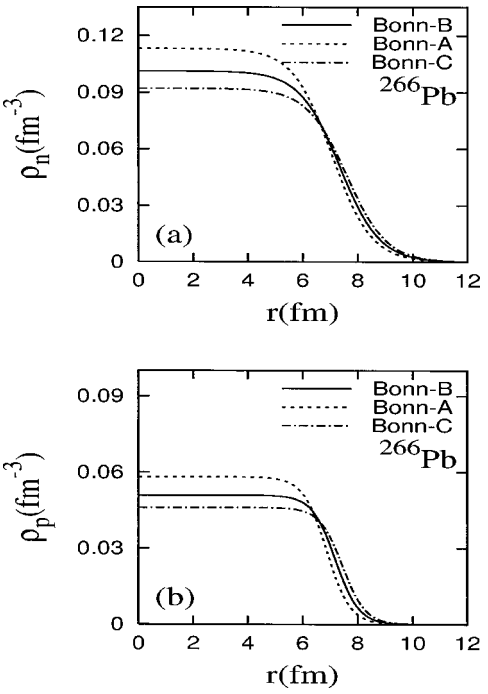

FIG. 6. As in Fig. 3, for ^{266}Pb.

Concerning neutron radii and skins, the empirical information available on them is unavoidably indirect, analyses being usually based on fits to proton scattering data. For ^{208}Pb, for instance, analyses of scattering data provide values of the neutron rms radius ranging from about 5.6 fm to 5.7 fm. The generally accepted range for the neutron skin is quoted as 0.16±0.02 fm, but values as large as 0.38 fm have been reported [2]. Most recently, Clark and collaborators [3] have found the neutron rms radius to be between 5.52 and 5.55 fm, and the neutron skin between 0.083 and 0.111 fm.

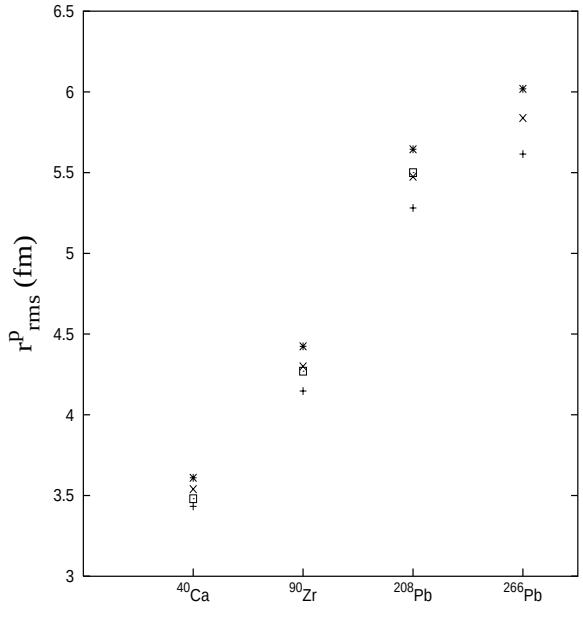

FIG. 7. Charge radii predicted with Bonn *A*(+), Bonn *B*(×), and Bonn *C*(*). The squares represent the experimental charge radii.

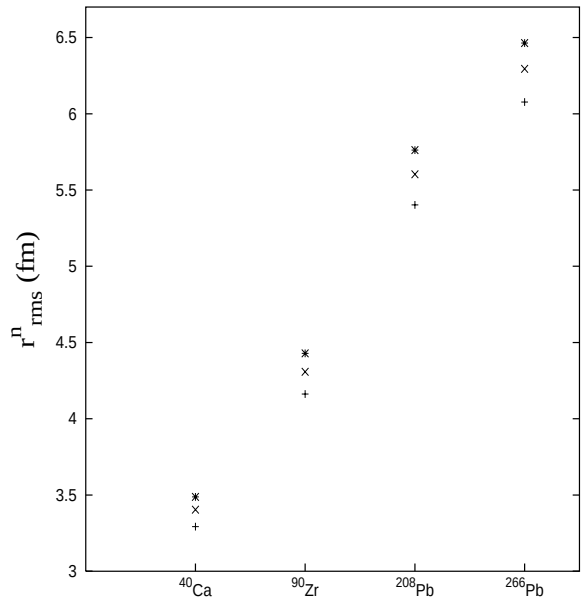

FIG. 8. Neutron rms radii predicted with Bonn $A(+)$, Bonn $B(\times)$, and Bonn $C(*)$.

Although in reasonable agreement with nonrelativistic Skyrme Hartree-Fock models, these are smaller than the generally accepted values we quoted above, including those from the present study, which are 5.60 fm for the neutron radius and 0.188 fm for the skin (with Bonn *B*).

Table II summarizes Bonn *B* predictions for charge radii, neutron radii, and skins. For comparison, some results from recent calculations are also included. For the charge radii, the values shown in the last column are from the relativistic Hartree calculation of Ref. [13]. For neutron radii and skins, the first entry in the last column refers to the analysis of Ref. [3], while the second entry gives the smallest and largest values from the analysis of Ref. [2]. Clearly, agreement (between analyses and theoretical predictions as well as among various analyses) is still elusive.

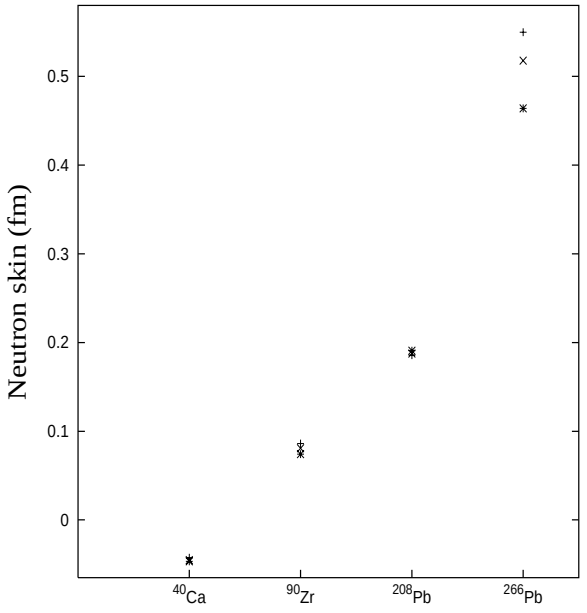

FIG. 9. Neutron skins predicted with Bonn $A(+)$, Bonn $B(\times)$, and Bonn $C(*)$.

Some experimental information specifically on neutron skins is also available for a few isotopic chains, but carries large uncertainties. In Fig. 10, our predictions obtained with Bonn *A*, *B*, and *C* for Sn isotopes are compared with the data of Krasznahorkay *et al.* [14]. The data were obtained from cross section measurements of isovector spin-dipole resonances excited by the $(^3\mathrm{He}, t)$ charge-exchange reaction at 450 MeV, and are not free of model assumptions [14]. Accurate determinations of neutron skins are obviously needed.

To conclude this section, we compare in Fig. 11 the predicted total matter densities (upper panel) and asymmetries $\alpha(r)$ (lower panel) for the ^{208}Pb and ^{266}Pb isotopes.

The central density is down by about 3% in ^{266}Pb, which we find to be consistent with the lower saturation density of asymmetric matter when α increases from about 0.2 to about 0.33 (see lower panel of Fig. 11).

C. A sample of nonrelativistic predictions

For completeness, we will also briefly mention some nonrelativistic calculations. In such cases, the input of Eq. (4) is the EOS as calculated in a conventional Brueckner-Hartree-Fock (BHF) calculation. We will show just one case, for the purpose of demonstration. Figure 11 displays the proton and neutron densities for ^{208}Pb calculated with the BHF framework in comparison with the DBHF predictions (Bonn *B* is used here). Nonrelativistic calculations imply central densities that are too high and radii that are unrealistically small. The proton and neutron (point) radii corresponding to Fig. 12 are 4.95 fm (corresponding to a charge radius of 5.01 fm) and 5.13 fm, respectively. We have observed very similar conclusions to apply to nonrelativistic calculations with more modern, high-precision interactions, such as CD-Bonn [15]. One must keep in mind that consideration of many-body forces is a crucial issue in nonrelativistic calculations, whereas some three-body forces are effectively included in the DBHF framework [16]. As it has been observed on many other occasions, the latter proves to be an effective and reliable method to describe microscopic interactions in the nuclear medium for both symmetric and asymmetric matter.

D. Further discussion

Before we proceed with our final summary and conclusions, we will take a closer look at our predictions in relation to the (symmetric) nuclear matter calculations of Ref. [17]. We also like to examine our findings with respect to the relative quality of the three potentials we apply (Bonn *A*, *B*, *C*) as seen through their reproduction of *NN* data.

First, we point out that our EOS calculations are moderately different from those reported in Ref. [17] using the same potentials, with our predictions showing more attraction. There are two sources of differences between our calculations and the ones of Ref. [17]. The first one is the absence of the two-nucleon center-of-mass momentum $(\vec{P})$ in the spinor normalization factors of our Eqs. (8) and (9) in Ref. [7].

TABLE II. Charge radii, point neutron radii, and neutron skins (in fm) predicted with Bonn *B*. When available, experimental values and/or results from recent studies are given. See text for details.

Nucleus	Observable	Experimental value	Bonn *B*	Other sources
^{40}Ca	r_{ch}	3.48	3.54	3.47[a]
	r_n		3.40	(3.310,3.314)[b]
	S_n		−0.0454	(−0.067, −0.063)[b]
^{90}Zr	r_{ch}	4.27	4.30	4.26[a]
	r_n		4.31	
	S_n		0.0809	
^{208}Pb	r_{ch}	5.50	5.47	5.49[a]
	r_n		5.60	(5.522,5.550),[b] (5.61,5.83)[c]
	S_n		0.188	(0.083,0.111),[b] (0.16,0.38)[c]
^{266}Pb	r_{ch}		5.84	
	r_n		6.30	
	S_n		0.518	

[a]Reference [13].
[b]Reference [3].
[c]Reference [2].

We leave this contribution out whereas the authors of Ref. [17] include it, but use the (untested) approximation $[(1/2)\vec{P}\pm\vec{K}]^2\approx(1/4)\vec{P}^2\pm\vec{K}^2$.

The second source of differences is in a technical aspect of the self-consistent calculation for the single-particle potential. The "effective mass ansatz" requires the choice of specific momenta at which the potential is to be evaluated, so that it can be fitted with a suitable analytic function. In contrast to what is done in Ref. [17], we reproduce the single-particle potential at momenta above the Fermi level, which we find more appropriate when using the continuous choice for the single-particle potential. By doing so we obtain effective masses that are larger (that is, closer to the free-space value), than those from Ref. [17]. (We adopted this point of view already a while ago in the context of proton-nucleus scattering calculations [18], where we noticed that "gentler" effective masses are more consistent with *p-A* scattering observables.)

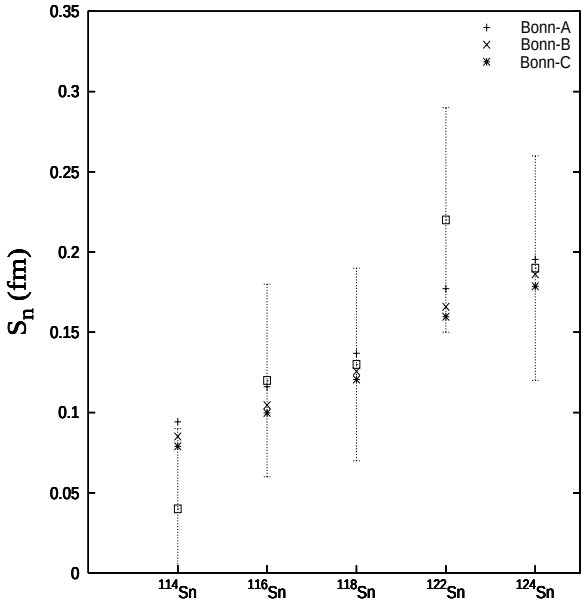

FIG. 10. Neutron skins predicted with Bonn *A*(+), Bonn *B*(×), and Bonn *C*(*) for Sn isotopes. Data from Ref. [14].

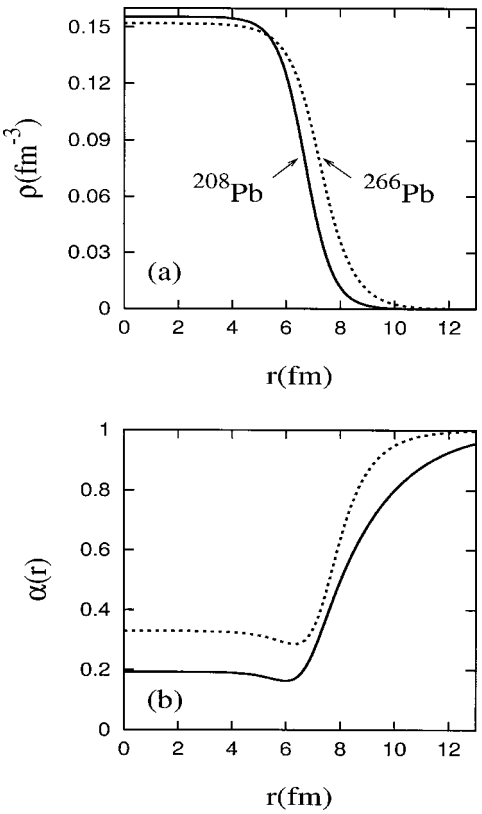

FIG. 11. Total matter density (a) and asymmetry (b) predicted with Bonn *B* for ^{208}Pb (solid line) and ^{266}Pb (dashed line).

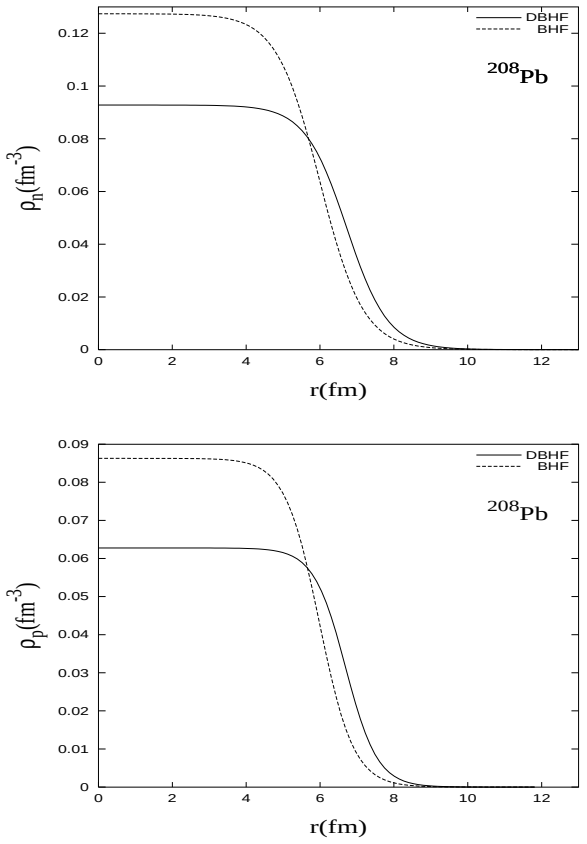

FIG. 12. Neutron (a) and proton (b) densities for ^{208}Pb predicted with a BHF calculation (dashed line) compared with the corresponding DBHF predictions (solid line).

Under the conditions described above, our study of nuclear energies and radii selects the Bonn *B* predictions as best, whereas it would be pointing at potential *A* had we done the EOS calculations exactly as in Ref. [17]. Either way, this work supports the conclusion that bulk observables such as energies and radii favor the EOS generated by potentials with low deuteron *D*-state probability P_D. It is generally true that ground state energies of nuclear few- and many-body systems are sensitive mainly to the deuteron *D*-state probability, and that a low P_D is necessary for sufficient binding.

Now, in the light of the above considerations, it is interesting to confront the aspect of quality of free-space predictions. In particular, can a low-P_D potential fit the ϵ_1 parameter correctly up to 300 MeV? Figure 5 of Ref. [17] suggests that this is only marginally possible. However, one must keep in mind that these potentials are relatively old. In the 1990s, potentials with high-precision fit to phase shifts were developed. (These high-precision potentials are nonrelativistic in nature and thus unsuitable for a DBHF framework, which is why we have chosen three relativistic, but older potentials, see comments in Sec. II C.)

Within the new generation of high-precision potentials, we notice that CD-Bonn has a P_D of 4.85% and fits the ϵ_1 parameter perfectly up to 350 MeV, thus showing that a simultaneous description of binding energies and *NN* scattering data is indeed possible.

III. SUMMARY AND CONCLUSIONS

We have presented calculations of nuclear energies, densities, and rms radii for some nuclei, ranging from symmetric to highly asymmetric. The main ingredient is the EOS from Ref. [7]. We use a mass formula as a simple yet direct tool to probe our EOS for infinite asymmetric matter in finite nuclei. Our predictions are essentially parameter free.

We compare with empirical information, when available. Realistic predictions for proton rms radii and binding energies are obtained if the EOS originates from DBHF calculations. An alternative popular approach is the use of a nonrelativistic framework together with phenomenological three-body forces.

Concerning the baseline force, the predictions obtained with Bonn *B* are best, reflecting a better balance of attraction and repulsion as compared to both Bonn *A* and *C*. (This issue has been examined closely in Sec. II D.)

The purpose of this paper was not to achieve the most accurate reproduction of empirical radii and energies, but rather to demonstrate that a microscopic density-dependent interaction based on realistic two-body forces and obtained within a DBHF description of asymmetric matter is capable of generating realistic predictions for both energies and radii without phenomenological adjustments, even if used in the simplest framework of a liquid drop model. The nuclei under consideration were chosen so as to sample different levels of asymmetries.

Our predictions for neutron radii and neutron skins are consistent with generally accepted values, which, on the other hand, are accompanied by large uncertainties. Additional theoretical work is clearly needed as well as accurate determinations of neutron densities. These may be available in the near future through parity violating measurements of neutron densities which have been proposed as a tool for measuring neutron distributions with unprecedented accuracy [19]. Parity violation arises from the interference of electromagnetic and weak amplitudes, with the Z^0 coupling mainly to neutrons at low Q^2. The data may be interpreted with as much confidence as electromagnetic scattering [19].

These measurements will provide more stringent constraints for theoretical models, as discussed in Ref. [19].

Our future plans include microscopic reaction studies with highly asymmetric nuclei. A proper account of the different proton and neutron distributions within a nucleus implies developing an α- and isospin-dependent effective interaction as discussed in Ref. [7]. We think the resulting effects could be important, even though the energy per particle in asymmetric nuclear matter is a very smooth function of α [7,20] and variations of α for most (familiar) nuclei tend to be small except near the skin. The main effect would indeed come from the isospin dependence of the interaction in those regions where variations of α are largest. Thus, following the asymmetry profile of a nucleus (for instance, shown in the lower panel of Fig. 10) with the appropriate interaction amounts to selecting the proper balance of $T=1$ and $T=0$ contributions, as determined by the relative proton/neutron densities. For instance, the interaction of, say, an incoming

neutron near the skin would be predominantly *nn*, and thus mostly $T=1$. This "isospin selection" could be important, especially for the more exotic topologies.

ACKNOWLEDGMENT

Financial support from the U.S. Department of Energy under Grant No. DE-FG03-00ER41148 is acknowledged.

[1] C. J. Horowitz and J. Piekarewicz, Phys. Rev. C **64**, 062802 (2001).
[2] S. Karataglidis, K. Amos, B. A. Brown, and P. K. Deb, Phys. Rev. C **65**, 044306 (2002).
[3] B. C. Clark, L. J. Kerr, and S. Hama, Phys. Rev. C **67**, 054605 (2003).
[4] R. J. Furnstahl, Nucl. Phys. **A709**, 85 (2002).
[5] K. Oyamatsu, I. Tanihata, Y. Sugahara, K. Sumiyoshi, and H. Toki, Nucl. Phys. **A634**, 3 (1998).
[6] T. Suzuki *et al.*, Phys. Rev. Lett. **75**, 3241 (1995).
[7] D. Alonso and F. Sammarruca, Phys. Rev. C **67**, 054301 (2003).
[8] See P. Danielewicz, R. Lacey, and W. G. Lynch, www.sciencexpress.org/31October2002/Page1/10.1126/science.1078070
[9] R. Machleidt, Adv. Nucl. Phys. **19**, 189 (1989).
[10] K. Oyamatsu, Nucl. Phys. **A561**, 431 (1993).
[11] B. A. Brown, Phys. Rev. C **58**, 220 (1998).
[12] D. Vautherin and D. M. Brink, Phys. Rev. C **5**, 626 (1972).
[13] F. Hofmann, C. M. Keil, and H. Lenske, Phys. Rev. C **64**, 034314 (2001).
[14] A. Krasznahorkay *et al.*, Phys. Rev. Lett. **82**, 3216 (1999).
[15] R. Machleidt, Phys. Rev. C **63**, 024001 (2001).
[16] G. E. Brown, W. Weise, G. Baym, and J. Speth, Comments Nucl. Part. Phys. **17**, 39 (1987).
[17] R. Brockmann and R. Machleidt, Phys. Rev. C **42**, 1965 (1990).
[18] F. Sammarruca, E. J. Stephenson, and K. Jiang, Phys. Rev. C **60**, 064610 (1999).
[19] C. J. Horowitz, S. J. Pollock, P. A. Souder, and R. Michaels, Phys. Rev. C **63**, 025501 (2001).
[20] L. Engvik, M. Hjorth-Jensen, and E. Osnes, Phys. Rev. Lett. **73**, 2650 (1994); L. Engvik, E. Osnes, M. Hjorth-Jensen, G. Bao, and E. Østgaard, Astrophys. J. **469**, 794 (1996).